

Static meson correlators in 2+1 flavor QCD at non-zero temperature

A. Bazavov¹ and P. Petreczky¹

Physics Department, Brookhaven National Laboratory, Upton, NY 11973, USA

Received: date / Revised version: date

Abstract. We study correlation functions of various static meson operators of size r at non-zero temperature in 2+1 flavor QCD, including Coulomb gauge fixed operators and Wilson loops with smeared spatial parts. The numerical calculations are performed on $24^3 \times 6$ lattices using highly improved staggered quark action. We discuss possible implications of our findings on the temperature dependence of the static energy of $Q\bar{Q}$ pair.

1 Introduction

At high temperature strongly interacting matter undergoes a transition to a new state called quark gluon plasma (QGP). Creating and exploring such state of matter is a subject of a large experimental program, see e.g. Ref. [1]. At the same time properties of strongly interacting matter at high temperatures can be studied in ab-initio calculations that rely on lattice regularization of QCD (see Ref. [2,3] for recent reviews).

The suppression of quarkonium production has been suggested by Matsui and Satz as probe of QGP formation in heavy ion collisions [4]. Interaction between heavy quark and anti-quark is expected to be modified by the deconfined medium at high temperature eventually leading to the dissociation of the quarkonium states. The suppression of the quarkonium yields in heavy ion collisions was indeed observed experimentally (see Ref. [5]). The interpretation of the experimental findings, however, requires the knowledge of quarkonium properties at high temperatures among other things (see Refs. [6,7,8] for recent reviews). Therefore there has been a significant effort to study in-medium properties of heavy quarkonium in recent years including lattice QCD studies. In-medium quarkonium properties are encoded in the spectral functions. A commonly used approach to obtain quarkonium spectral functions relies on lattice QCD calculation of the correlation functions in Euclidean time direction and extraction of the quarkonium spectral functions using the Maximum Entropy Method [9,10,11,12,13,14]. However, it turns out that temporal quarkonium correlators are remarkably insensitive to the in-medium modification of the corresponding spectral functions due to the limited extent of the imaginary time direction $\tau < 1/(2T)$ [15]. The dissolution of the bound state peaks in the spectral functions is compensated by large enhancement of the spectral function in the threshold region in such a way that cor-

responding Euclidean correlation functions do not change significantly for $\tau < 1/(2T)$ [16]. This picture is corroborated by the study of the spatial charmonium correlation functions [17]. Unlike temporal correlators spatial correlators can be calculated for separation larger than $1/(2T)$ and show strong temperature dependence consistent with dissolution of the bound states [17].

Because of the above problems the calculation of the quarkonium spectral functions from finite temperature Euclidean time correlation functions is very difficult. An alternative approach is to calculate quarkonium spectral functions relies on effective theories. Quarkonium is characterized by three different energy scales: the heavy quark mass m , the inverse quarkonium size $1/r \sim mv$ and the quarkonium binding energy mv^2 . Integrating out the largest energy scale $\sim m$ leads to an effective theory called non-relativistic QCD (NRQCD). This effective theory was combined with lattice QCD method to study quarkonium properties both at zero [18] and non-zero temperatures [19, 20]. Integrating out the scale mv gives an effective theory called potential non-relativistic QCD (pNRQCD) [21,22]. The Lagrangian of pNRQCD is formulated in terms of singlet and octet fields of the heavy quark anti-quark pair and the heavy quark potential enters as the parameter of the effective Lagrangian. At non-zero temperature additional scales T and gT appear. Depending on how these scales are related to the above energy scales the heavy quark potential may be modified by the medium accordingly [23]. At non-zero temperature the potentials also have an imaginary part [23,24]. The above effective field theory approach is based on the weak coupling, namely on the assumption that $mv, T, gT \gg \Lambda_{QCD}$. Within this framework in-medium quarkonium properties can be calculated [25] and one can also take the static limit and calculate the energy of a static $Q\bar{Q}$ pair which like the potential also has an imaginary part.

It is not clear if in the interesting temperature range the above scale separation holds. However, we may expect that the binding energy of quarkonium states is reduced with increasing temperature. Close to the dissolution point the binding energy is the smallest scale in the problem and all other scales, including Λ_{QCD} can be integrated out. In that regime the potential of the corresponding effective theory is equal to the energy of $Q\bar{Q}$ pair [26]. Therefore calculation of the static energy at non-zero temperature in the non-perturbative region could be very helpful for the determination of in-medium quarkonium properties.

At zero temperature the energy of static $Q\bar{Q}$ pair is calculated by studying correlation function of static meson operators at large Euclidean time separations. This is not possible at non-zero temperature due to the limited temporal extent $\tau \leq 1/T$. It has been suggested to extract the static quark potential at non-zero temperature from the spectral representation of the simplest finite temperature static meson correlators, namely rectangular Wilson loops and MEM [27,28]. The analysis was performed in quenched approximation. In this paper we are going to analyze the temperature dependence of correlation functions of various static meson operators in 2+1 flavor QCD across the chiral crossover region and discuss its implication for the temperature dependence of the static $Q\bar{Q}$ energy. Apart from quantitative determination of the static energy at non-zero temperature the study of static meson correlators is interesting because they are simpler than quarkonium correlators and can provide some insight into the inter-quark interaction in the medium and the weakly interacting nature of QGP. One of the aims of the present study is to find out to what extent the temperature dependence is influenced by the choice of the interpolating meson operator. Obviously only the features that are not sensitive to the specific choice of the meson operators are of some relevance. Some preliminary results have been reported in conference proceedings [29,30].

2 Static quark anti-quark correlators in lattice QCD

Let us consider a static meson operator of the form

$$O(x, y; \tau) = \psi^\dagger(x, \tau) U(x, y; \tau) \psi(y, \tau). \quad (1)$$

Here ψ and ψ^\dagger are the static quark and anti-quark fields, and $U(x, y; \tau)$ is the spatial Wilson line connecting points x and y . After integrating out the static quark anti-quark fields the correlation function of this operator at time τ becomes the well known Wilson loop of size $r \times \tau$ (see e.g. Ref. [31]). One can also fix the Coulomb gauge and omit the spatial Wilson line $U(x, y; \tau)$. In this case one gets correlation function of two Wilson lines of extent τ . The static meson correlation function has the following spectral representation [31]

$$G(r, \tau) = \sum_{n=1}^{\infty} c_n(r) \exp(-E_n(r)\tau), \quad r = |x - y|. \quad (2)$$

The coefficients c_n depend on the choice of the operator, while the energy levels $E_n(r)$ corresponding to all possible states containing static quark and anti-quark do not [31]. If truncated to include some number of terms, the above spectral representation can in principle be used to determine the energy levels of $Q\bar{Q}$ states in QCD at zero temperature. The lowest energy level of $Q\bar{Q}$ pair is commonly referred to as the static potential, while the higher energy levels are called the hybrid potentials. At sufficiently high temperatures, however, Eq. (2) is of little use since $\tau \leq 1/T$ and one has to consider infinite number of terms in Eq. (2). As mentioned above at finite temperature the energy of a static $Q\bar{Q}$ pair has also an imaginary part. It is not clear how this imaginary part would manifest itself in the Euclidean correlation function. It was suggested to generalize the spectral representation of the static meson correlators in terms of a temperature dependent spectral function [27,28]

$$G(r, \tau) = \int_{-\infty}^{\infty} d\omega \sigma_r(\omega, T) e^{-\omega\tau}. \quad (3)$$

At zero temperature Eq. (2) and Eq. (3) are equivalent and the spectral function $\sigma(\omega, T)$ is just the sum of delta functions. The imaginary part of the static energy now is encoded in the width of the spectral function. While the spectral function $\sigma_r(\omega, T)$ depends on the choice of the meson operator $O(x, y; \tau)$, the peak position and its width will not as long as there is a well defined bound state peak. Another way to arrive at Eq. (3) is to consider the correlation function of static meson operators in real time

$$D^>(t) = \text{Tr}(O(t)O(0) \exp(-\beta H)) = \int_{-\infty}^{\infty} \frac{d\omega}{2\pi} \exp(-i\omega t) D^>(\omega) \quad (4)$$

and then continue to imaginary time $D^>(t) \rightarrow D^>(-i\tau)$. Using the standard definition of the spectral function

$$\sigma_r(\omega, T) = \frac{D^>(\omega) - D^<(\omega)}{2\pi} \quad (5)$$

and recalling that $D^< = 0$ in the case of static quarks (see discussions in Ref. [23]) we get Eq. (3). Note, that unlike quarkonium spectral function $\sigma_r(\omega)$ is not odd function of ω . From the point of view of MEM reconstruction of the spectral function $\sigma_r(\omega, T)$ from Eq. (3) is not much different from the reconstruction of the quarkonium spectral functions. However, the structure of the spectral function in the static case could be simpler and the cancellation of the temperature effects in the correlation function due to subtle interplay between the bound state peak and the continuum is not expected to happen. As a result we should see a more pronounced temperature dependence of the correlation functions. The above discussion holds for $\tau < 1/T$. The case $\tau = 1/T$ should be considered separately because it is related to the free energy of static $Q\bar{Q}$ pair.

The correlation function evaluated at the maximal Euclidean time extent gives the so-called singlet free energy $F_1(r, T) = -T \ln G(r, \tau = 1/T)$. The singlet free

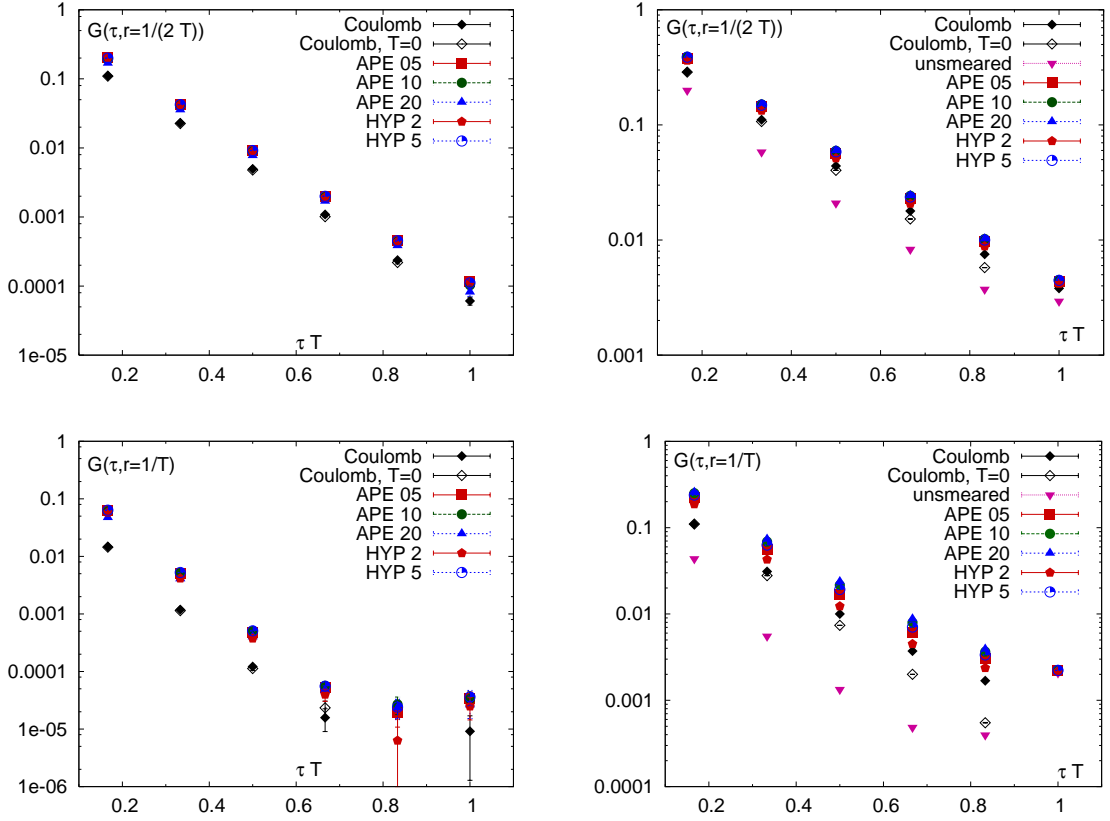


Fig. 1. Static meson correlators as function of τ for two spatial separations: $rT = 1/2$ (upper panels) and $rT = 1$ (lower panels). The numerical results are shown for two temperatures $T = 147$ MeV (left) and $T = 266$ MeV (right).

energy has been studied in the past in pure gauge theory [32,33,34,57,35,36] and in QCD [37,38,39,40]. Most of these studies use Coulomb gauge correlators but in Refs. [32,36] also Wilson loops have been considered. Unlike the true free energy of a static quark anti-quark pair $F(r, T)$, defined in terms of Polyakov loop correlators, $F_1(r, T)$ depends on the choice of the gauge or the choice of $U(x, y; \tau)$ and thus is not physical. However, in the limit of the infinite separation it gives the $Q\bar{Q}$ free energy $F_\infty(T) = \lim_{r \rightarrow \infty} F(r, T) = \lim_{r \rightarrow \infty} F_1(r, T)$. The singlet free energy is gauge independent in hard thermal loop (HTL) approximation [41] and coincides with the real part of the static energy in this approximation [24,23]. The singlet free energy also arises in the context of short distance, $rT \ll 1$ behavior of the Polyakov loop correlator and its decomposition into singlet and octet contribution within the pNRQCD framework [42]. Here it is defined as the singlet field correlator and thus is independent of $U(x, y; \tau)$ or gauge fixing. It is equal to the zero temperature static potential up to power corrections, which are well defined and calculable at any order of perturbation theory. The singlet free energy defined in Coulomb gauge or in terms of rectangular (unsmeared) Wilson loops was studied using resummed HTL perturbation theory [43]. This calculation revealed that new type of temperature dependent divergences, so-called intersection divergences

appear in the case of Wilson loops. These divergences have been shown to arise due to mixing of cyclic Wilson loops with the Polyakov loop correlators [44] and can be removed if a proper renormalization procedure is implemented. This should make a quantitative comparison of the perturbative results with lattice data on the singlet free energy possible, thus providing a stringent test of the weakly interacting nature of QGP.

3 Numerical results

3.1 Lattice approach and parameters

We calculated static meson correlation functions on $24^3 \times 6$ lattice. Because of relatively small N_τ small statistical errors can be achieved. The gauge configurations used in our study have been generated by the HotQCD collaboration using a combination of the tree-level improved gauge action and Highly Improved Staggered Quark (HISQ) action [45]. This combination of the gauge action and quark action was referred to as the HISQ/tree action in Ref. [45] but here we refer to it as the HISQ action for simplicity. The Highly Improved Staggered Quark action was first discussed in Ref. [46]. The gauge configurations have been generated using rational hybrid Monte-Carlo algorithm

Table 1. Parameters of the lattice calculations

β	m_s	T [MeV]	# TU
6.000	0.1138	147	27000
6.050	0.1064	155	30000
6.100	0.0998	162	30000
6.150	0.0936	170	30000
6.195	0.0880	178	30000
6.285	0.0790	194	30000
6.423	0.0670	223	30000
6.575	0.0564	258	30000
6.608	0.0542	266	30000
6.664	0.0514	281	30000
6.800	0.0448	320	7000
6.950	0.0386	368	7480
7.150	0.0320	442	4770
7.280	0.0284	488	4310

[47]. The algorithmic details of dynamical HISQ simulations can be found in Ref. [48]. The simulations have been performed for the physical value of the strange quark mass m_s and light quark masses $m_l = m_s/20$. This light quark mass corresponds to the pion mass of 160 MeV in the continuum limit [45]. The parameters of the lattice simulations including the lattice gauge coupling $\beta = 10/g^2$ and the strange quark mass in lattice units are shown in Table 1 along with the corresponding temperatures. As one can see from the table we consider a wide temperature range across the chiral crossover, which for $N_\tau = 6$ occurs at $T_c = 171(1)$ MeV [45]. The last column of the table shows the accumulated statistics for each β value in terms of molecular dynamics time units (TU). Static meson correlators have been calculated after each 10 TUs. The lattice spacing a is determined from the r_1 parameter defined in terms of the zero-temperature static potential as

$$r^2 \frac{dV}{dr} \Big|_{r=r_1} = 1.0, \quad (6)$$

and we use the value $r_1 = 0.3106$ fm [49]. We use the parameterization of the lattice spacing and the quark masses as functions of the gauge coupling β along the lines of constant physics that are given in Ref. [45].

Typically in lattice calculations a straight line path is used in the definition of the static meson operator in Eq. (1), i.e. rectangular Wilson loops being calculated on the lattice. The main problem with calculating rectangular Wilson loops on the lattice and extracting potential from them is the large noise. To reduce the noise and improve the signal for the ground state potential smeared gauge links are used. The simplest example of smeared gauge links is the well known APE smearing [50]. In this case a 3-link staple is added to each elementary lattice gauge link with some coefficient and the resulting sum is projected to SU(3) gauge group. Another smearing called hyper-cubic or HYP smearing was introduced in Ref. [51]. In this case the smeared links are constructed from APE smeared links in lower dimensional subspace, such that the entire construction of the smeared links stays within the hypercube

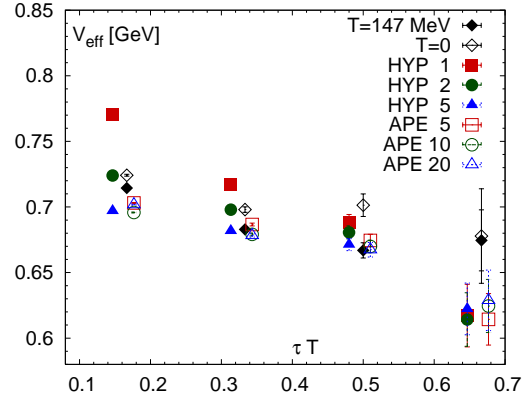


Fig. 2. The effective potential for $rT = 1/2$ as function of τ at the lowest temperature $T = 147$ MeV. The open and filled diamonds correspond to Coulomb gauge correlators at zero and non-zero temperature, respectively.

[51]. This smearing procedure depends on 3 parameters in 4 dimensions, one for each level of APE smearing. Both APE and HYP smearing can be applied iteratively to increase the signal to noise ratio. Typically several steps of APE and HYP smearing are used. The HYP smearing turned out to be more efficient than the APE smearing in the calculations of the static potential in pure gauge theory [51]. The APE smearing was used in calculating the static potential in 2+1 flavor QCD (see e.g. [52, 53]), while HYP smearing was used for example in Refs. [54]. An alternative approach to reduce the noise in the calculations of the static potential is to fix the Coulomb gauge (see e.g. [45, 55]). Both approaches turned out to be equally efficient.

In the present study we calculated static meson correlators $G(\tau, r)$ at non-zero temperature using smeared spatial gauge links as well as Coulomb gauge. The smearing of the gauge links was restricted to spatial directions only, i.e. no temporal links enter the construction of the smeared links. We used several iterations of APE and HYP smearing. The coefficient of the staple for the APE smearing was $c = 0.4$, while for the HYP smearing we used the same smearing parameters as in Ref. [51], i.e. $\alpha_2 = 0.3$ and $\alpha_3 = 0.6$ in the notation of Ref. [51]. The parameter α_1 does not enter because we consider spatial directions only. We used 5, 10 and 20 iterations of APE smearing and 1, 2 and 5 iterations of HYP smearing.

3.2 Time dependence of static correlators

As the first step toward understanding the temperature dependence of the static energy one should examine the τ -dependence of static meson correlators for various temperatures and different spatial separations r . As the medium effects on static meson correlators are expected to depend on how r and τ compare to the inverse temperature we will scale these variables by the temperature when presenting our numerical results. Our numerical results for the static meson correlators as function of τ with different

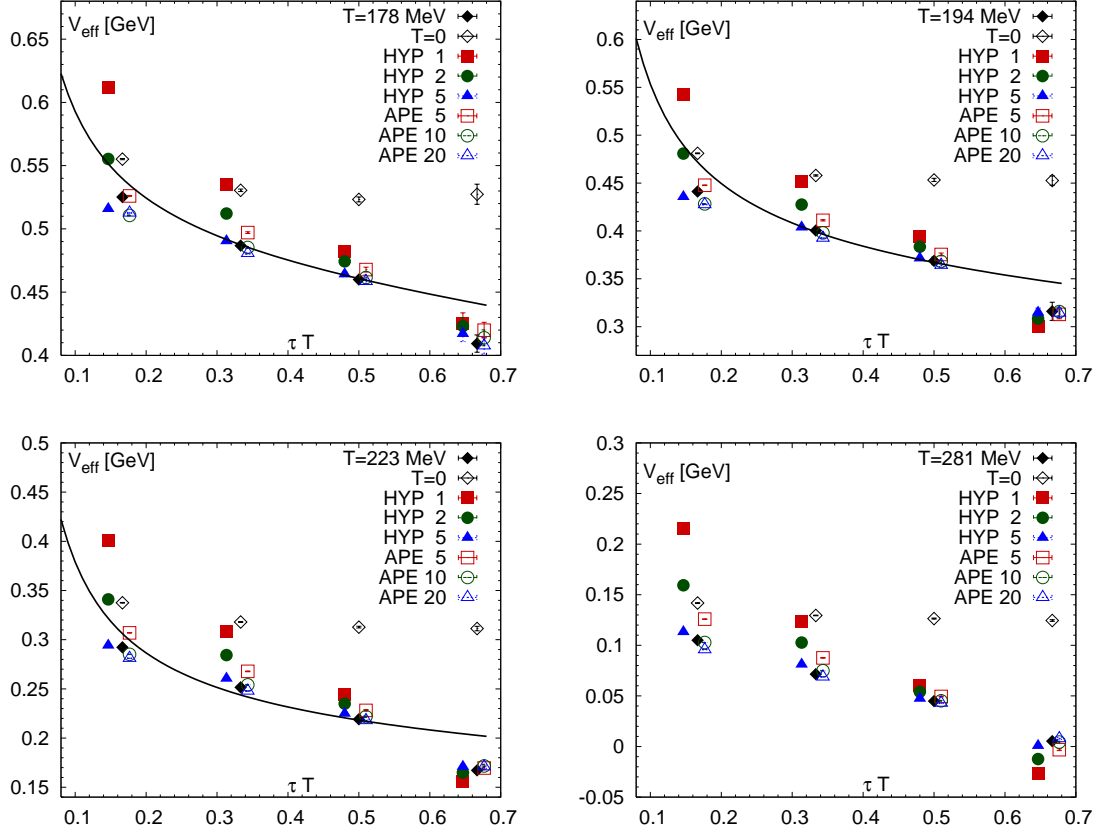


Fig. 3. The effective potential corresponding to various correlators at different temperatures for $rT = 1/2$ as function of τ . The open and filled diamonds correspond to Coulomb gauge correlators at zero and non-zero temperature, respectively.

smear links as well as for Coulomb gauge are shown in Fig. 1 for two spatial separation $rT = 1/2$ and $rT = 1$. We also compared our results with zero temperature results obtained in Coulomb gauge [45]. Note that unlike quarkonium correlators static meson correlators are not subject to periodic boundary conditions and thus can be studied also for $\tau T > 1/2$. As expected we see significant in-medium modification of the static meson correlators in contrast to quarkonium correlators. The modifications become larger with increasing r and increasing temperature: they are negligible at $rT = 1/2$, $T = 147$ MeV and are the largest for $rT = 1$ and $T = 266$ MeV. While the correlators in Coulomb gauge and smeared Wilson loops appear to be similar, unsmeared Wilson loops show quite different behavior. They appear to have more curvature as function of τ and also have a different slope. One of the most prominent features of the finite temperature data is that the static meson correlator does not seem to follow an exponential decay at large τ but flattens off or slightly increase around $\tau T \simeq 1$.

The increase around $\tau T \simeq 1$ can be interpreted as a small contribution to the spectral function $\sigma(\omega)$ at negative frequencies which arises due to periodic boundary conditions on the gluon background even-though static quarks propagate only forward in time, i.e. correspond to positive frequency. At least such interpretation seems to

be supported by MEM analysis of Wilson loops [28] and bottomonium correlators obtained in NRQCD [19]. Another way to understand the increase of the spatial meson correlator at $\tau T = 1$ is to inspect the HTL resummed perturbative result for rectangular Wilson loop [24]. The resummed 1-loop correction to the rectangular Wilson loop consist of three terms: a term linear in τ that is proportional to the real part of the potential, a constant term and a term periodic in τ [24]. After a proper re-exponentiation the term linear in τ will correspond to the exponentially decaying part, while the two other terms can explain the behavior at $\tau T \simeq 1$.

While different correlators have different behavior in τ they all converge at a similar value for $\tau T = 1$. For very large distances in fact this is expected, as $-T \ln G(\tau = 1/T, r)$ gives the free energy of static quark anti-quark pair and therefore all correlators should be equal (see the discussion in the previous section). The convergence of different correlators for $rT = 1$ is due to strong screening effects, i.e. the fact that $-T \ln G(\tau = 1/T, r)$ is not very different from F_∞ .

At zero temperature the large τ behavior of $G(r, \tau)$ is dominated by the static potential. Therefore it is customary to study the effective potential defined in terms of the

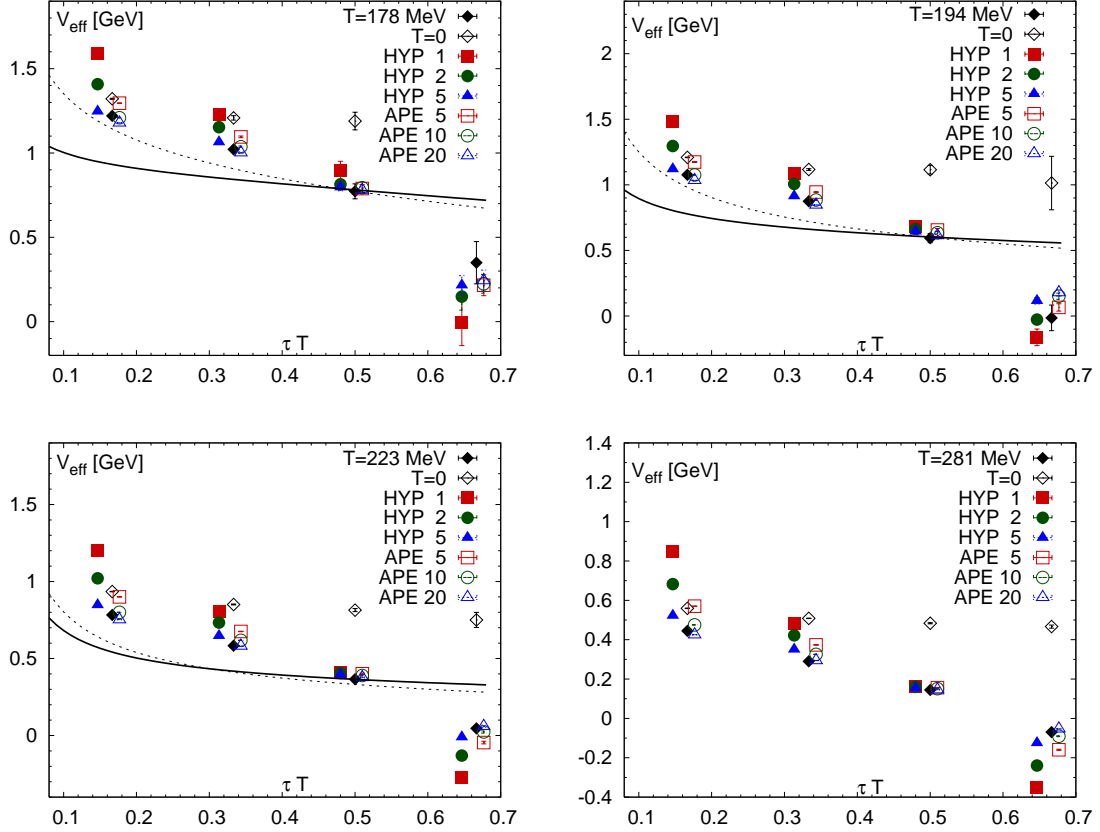


Fig. 4. The effective potential corresponding to various correlators at different temperatures for $rT = 1$ as function of τ . The open and filled diamonds correspond to Coulomb gauge correlators at zero and non-zero temperature, respectively.

following ratio

$$aV_{eff}(r, \tau) = \ln \frac{G(r, \tau/a)}{G(r, \tau/a + 1)}. \quad (7)$$

Here a denotes the lattice spacing. The effective potential is expected to decrease with increasing τ , eventually reaching a plateau that corresponds to the value of the static potential. How quickly V_{eff} reaches a plateau depends on the choice of the static meson operator in Eq. (1), using more smearing in the gauge connection $U(x, y; \tau)$ typically suppresses the contribution from the excited states. Using the Coulomb gauge is also an effective method for suppressing the excited state contributions. The effective potential turns out to be a useful tool to examine the behavior of the static meson correlators in more detail. In Fig. 2 we show our numerical results for V_{eff} calculated for different smearing of the spatial links as well as for Coulomb gauge for the lowest temperature of 147 MeV and distance $rT = 1/2$. We do not show V_{eff} from unsmeared Wilson loops as the corresponding numerical results are too noisy. We compare our numerical results with the zero temperature results in Coulomb gauge [45] which approach a plateau within the considered τ range. At the lowest temperature we do not expect large modification of the static potential. Indeed the temperature effects on V_{eff} are small for $\tau T < 1/2$ and indicate a

downward shift of the static potential of about 10 MeV. This is consistent with the study of the static potential in pion matter, where a similar downward shift has been observed [54] (see also Ref. [56] for a related study for quarkonium). The figure also shows that Coulomb gauge results and smeared Wilson loops give similar results if sufficient number of smearings steps is used, i.e. 5 or more smearing steps in the case of APE smearings and more than two steps for HYP smearings. For one or two steps of HYP smearings the excited state contribution, seen as the curvature at small τ , is significant. While the effective potential reaches a plateau at zero temperature within the studied τ -range, this is not the case for the lowest temperature. The decrease in V_{eff} at $\tau T = 2/3$ is particularly striking and difficult to explain in terms of the expected in-medium modifications of the static energy. Similar results have been obtained for $T = 155$ MeV, 162 MeV and 178 MeV.

Now let us discuss the behavior of V_{eff} above the chiral transition temperature. We show our numerical results for $rT = 1/2$ and $rT = 1$ in Fig. 3 and Fig. 4, respectively. The features of V_{eff} discussed above also hold at higher temperatures, in particular, V_{eff} does not show a plateau and there is a rapid decrease around $\tau T = 2/3$. The effective potential above T_c is always smaller than the $T = 0$ result and the deviations increase with increasing

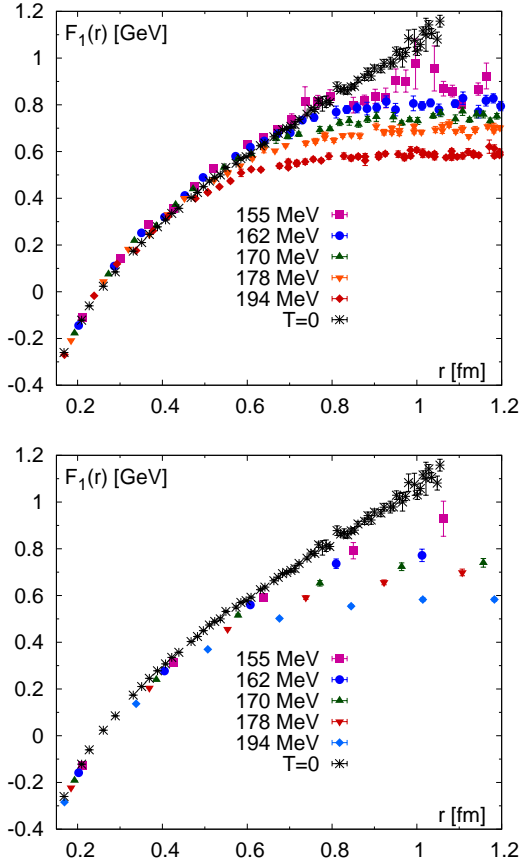


Fig. 5. The singlet free energy as function of distance r for different temperatures $T < 200$ MeV calculated in Coulomb gauge (top) and using smeared Wilson loops with 5 steps of HYP smearing (bottom). We also show the zero temperature static potential for $\beta = 6.664$ [45].

temperatures and distance suggesting that the static potential decreases with increasing temperature. Note that we do not present our results for V_{eff} from unsmeared Wilson loops as these show much stronger τ -dependence and would change the scale of Figs. 3 and 4 substantially.

At temperatures significantly higher than the transition temperature we expect the imaginary part of the potential to play an important role. Therefore it is natural to ask whether the above features of V_{eff} are due to the imaginary part. According to thermal pNRQCD the spectral function defined in terms of $D^>$, i.e. $\sigma_r = D^>(\omega)/(2\pi)$ has the Breit-Wigner form [23]

$$\sigma_r(\omega) = \frac{1}{\pi} \frac{\text{Im}V}{(\omega - \text{Re}V)^2 + \text{Im}V^2} \quad (8)$$

(c.f. Eq. (96) in Ref. [23]). To model the effects of $\text{Im}V$ on the effective potential we calculated the static correlators using the above form for the spectral function and Eq. (3) together with some plausible values of $\text{Im}V$ inspired by weak coupling calculations. The r -dependence of the imaginary part of the potential is quite complicated even in the weak coupling regime. For large r , however, it has

a simple form $C_F \alpha_s m_D$, while it vanishes for $rT \ll 1$. For the relevant temperature range $\alpha_s m_D \sim 1$. Therefore in our modeling efforts we assume that $\text{Im}V = T$ for $rT = 1$ and $\text{Im}V = T/2$ for $rT = 1/2$. The value of $\text{Re}V$ was adjusted to match the value of V_{eff} at $\tau T = 1/2$. The corresponding results are shown in Figs. 3 and 4 as solid black lines. For $rT = 1$ we also allow for a larger value of the imaginary part of the potential, namely $\text{Im}V = 3T$. The corresponding results are shown as the dashed lines in Figs. 3 and 4. As one can see from the figures the τ dependence of V_{eff} in general is not described well by the above form of the spectral function. For $rT = 1/2$ the Breit-Wigner form captures some features of the τ dependence but for $rT = 1$ the observed curvature of V_{eff} is much larger than the one that can be provided by the Breit-Wigner form, even if we assume that $\text{Im}V = 3T$. The Breit-Wigner form describes the spectral function well in the vicinity of the pole. For large values of $\text{Im}V$ the Breit-Wigner form has long tails that extend to the ω regions where the form is not valid, e.g. Eq. (8) obtained from pNRQCD is not valid for large values of ω . Therefore we also consider a Gaussian Ansatz with the same width as used in the Breit-Wigner form and calculate $G(r, \tau)$. In this case we get very small τ -dependence of V_{eff} . Thus the τ dependence seen in Figs. 3 and 4 for the Breit-Wigner form is generated by its tails. Therefore it seems unlikely that the τ -dependence of V_{eff} is due to the imaginary part of the static potential, instead there could be an additional contribution to the static correlator that arises from the periodic boundary.

As discussed above, based on HTL resummed results we expect that Wilson loops at high temperatures will consist of two contributions: one exponentially decaying in τ and another one with more complex τ behavior. Therefore we tried to fit the τ dependence of the static correlators by a simple form

$$A \exp(-\tilde{V}\tau) + c \exp(-\Delta(1/T - \tau)) \quad (9)$$

for $1/2 \leq \tau \leq 2/3$. The fit form works well but the extracted value of \tilde{V} depends somewhat on the chosen fit range. However, it is always smaller than the $T = 0$ static potential. This together with the analysis of V_{eff} suggests that the energy of static $Q\bar{Q}$ pair is decreasing with increasing temperature contrary to the results obtained in Ref. [28] based on calculations in SU(3) gauge theory and MEM. We also find that the non-exponential contribution is relatively small. Namely we find that c is about 1000 times smaller than A , however, it increases with increasing temperature.

3.3 Singlet free energy

As discussed in section 2 $F_1(r, T) = -T \ln G(r, T)$ gives the singlet free energy of static $Q\bar{Q}$. We have calculated the singlet free energy F_1 using Coulomb gauge and smeared as well as unsmeared Wilson loops. We start the discussion of our numerical results first considering the low temperature region $T < 200$ MeV. This region of course also

contains temperature values above the chiral crossover. Our results for Coulomb gauge and smeared Wilson loops are shown in Fig. 5 and compared to the zero temperature static energy calculated in Ref. [45] at $\beta = 6.664$. We do not show the results from unsmeared Wilson loops because they are too noisy. It is suffice to say that they are above the Coulomb gauge result. All the smeared Wilson loops give very similar results for F_1 , i.e. the details of smearing do not seem to matter. The singlet free energy does not show a significant change across the chiral crossover and the temperature effects are relatively small for $r < 0.65$ fm. In the case of Coulomb gauge F_1 is slightly larger than the zero temperature static potential at intermediate distances $0.3 \text{ fm} < r < 0.8 \text{ fm}$. This is qualitatively similar to the findings in pure gauge theory [34,36,57]. As discussed in Ref. [36] this is due to the fact that $c_1 < 1$. In the case of smeared Wilson loops F_1 is always smaller than the zero temperature static energy since c_1 is expected to be close to unity [36].

Our results for the high temperature region, $T > 200$ MeV are shown in Fig. 6 for Coulomb gauge and unsmeared Wilson loops. As expected at very small distances F_1 is temperature independent and coincides with the $T = 0$ potential. For $T > 200$ MeV the numerical results for unsmeared Wilson loops have quite small statistical errors. Therefore one can use our numerical results to test the perturbative predictions for cyclic Wilson loops [43,44]. Note that for Coulomb gauge the singlet free energy does not overshoot the zero temperature static potential similarly to the case of pure gauge theory [34,57,36]. This may imply that the coefficients c_n are not important for the temperature dependence of F_1 at high temperatures. As the temperature increases the singlet free energy reaches the plateau at smaller and smaller distances consistent with expectations based on color screening. Figure 6 shows that F_1 obtained from unsmeared Wilson loops is systematically larger than F_1 obtained in Coulomb gauge at intermediate distances. This could be due to the intersection divergences of cyclic Wilson loops [44]. Smeared Wilson loops on the other hand give results which are slightly smaller than Coulomb gauge results at intermediate distances, except for one iteration of HYP smearing. There is no dependence on the smearing if more than one smearing steps are used. To make this point clear in Fig. 7 we compare F_1 obtained for different correlators at $T = 281$ MeV. Similar results have been obtained at other temperatures.

To explore the large distance behavior of the singlet free energy we consider the following combination

$$S_1(r, T) = -r(F_1(r, T) - F_\infty(T)). \quad (10)$$

At leading order this combination should decay exponentially and its exponential decay is governed by the leading order Debye mass $m_D^{LO} = gT\sqrt{3/2}$. The perturbative analysis of F_1 quantity at next-to-leading order was first performed in Ref. [43] and in the case of Coulomb gauge revealed a power-law behavior. However, as mentioned already the renormalization of the static meson correlators at $\tau = 1/T$ is non-trivial. We find that $S_1(r, T)$ decays

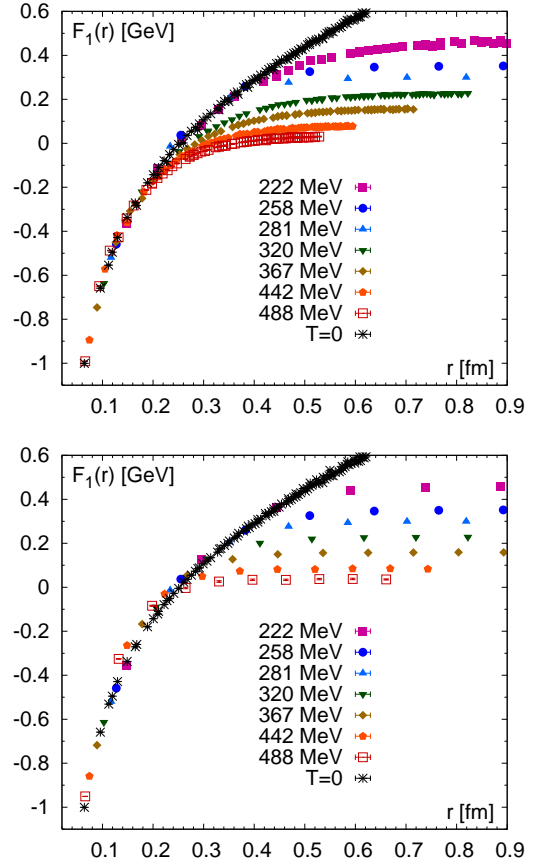


Fig. 6. The singlet free energy as function of distance r for different temperatures $T > 200$ MeV calculated in Coulomb gauge (top) and using unsmeared Wilson loops (bottom). We also show the zero temperature static potential for $\beta = 6.664$ and $\beta = 7.28$ [45].

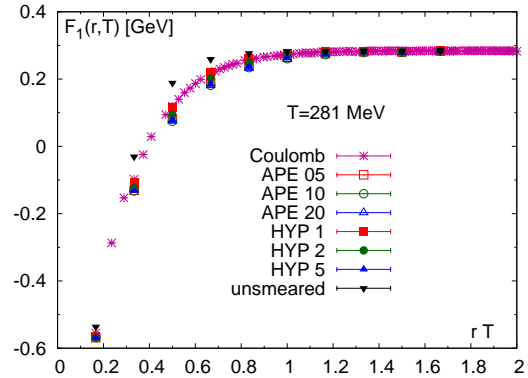


Fig. 7. The singlet free energy at $T = 281$ MeV defined in Coulomb gauge and in terms of different Wilson loops.

exponentially for $r > 1/T$. The corresponding screening mass \tilde{m}_E/T shows only mild temperature dependence for $T > 300$ MeV consistent with expectations. Furthermore, we find that \tilde{m}_E/T for unsmeared Wilson loops is significantly larger than for Coulomb gauge. The screening masses obtained from smeared Wilson loops are similar or slightly smaller than the ones obtained in Coulomb gauge. The only exception is the case when one iteration of HYP smearing is used, where m_E/T is closer to the value obtained from unsmeared Wilson loops.

4 Conclusions

In this paper we studied various static meson correlators at non-zero temperature. We analyzed the temperature dependence of these correlators as well as their dependence on the Euclidean time τ . The τ -dependence of the correlators has been analyzed in terms of the effective potential V_{eff} for various spatial separations r . For large Euclidean times V_{eff} gives the static potential in the zero temperature case. We found that static meson correlators defined in Coulomb gauge and in terms of smeared Wilson loops show quite similar behavior. Contrary to the zero temperature case the effective potential does not reach a plateau in the studied τ window even at the lowest temperatures. We explored different possibilities to explain this behavior including the presence of an imaginary part of the static energy. We conclude that this behavior is due to the additional contribution not related to the static potential that arises from the periodic boundary condition. To extract the potential at non-zero temperature we will need to extend this calculation to larger N_τ . We also calculated the singlet free energy and found that its behavior is qualitatively similar to the previous findings obtained in pure gauge theory. Comparing our numerical results with perturbative prediction on F_1 [42,43,44] will be useful to clarify the strongly or weakly interacting nature of the QGP.

Acknowledgments

This work was supported by U.S. Department of Energy under Contract No. DE-AC02-98CH10886. The numerical simulations have been performed at NERSC and on BlueGene/L computers at the New York Center for Computational Sciences (NYCCS) at Brookhaven National Laboratory. We would like to thank A. Rothkopf for valuable discussions on the behavior of Wilson loops at $\tau T \simeq 1$.

References

1. B. Muller, J. L. Nagle, Ann.Rev.Nucl.Part.Sci. **56**, 93 (2006), nucl-th/0602029
2. O. Philipsen (2012), 1207.5999
3. P. Petreczky, J.Phys. **G39**, 093002 (2012), 1203.5320
4. T. Matsui, H. Satz, Phys. Lett. **B178**, 416 (1986)
5. R. Granier de Cassagnac, J.Phys. **G35**, 104023 (2008), 0806.0046
6. A. Mocsy, P. Petreczky, M. Strickland (2013), 1302.2180
7. N. Brambilla, S. Eidelman, B. Heltsley, et al., Eur.Phys.J. **C71**, 1534 (2011), 1010.5827
8. R. Rapp, D. Blaschke, P. Crochet, Prog.Part.Nucl.Phys. **65**, 209 (2010), 0807.2470
9. T. Umeda, K. Nomura, H. Matsufuru, Eur. Phys. J. **C39S1**, 9 (2005), hep-lat/0211003
10. M. Asakawa, T. Hatsuda, Phys. Rev. Lett. **92**, 012001 (2004), hep-lat/0308034
11. S. Datta, F. Karsch, P. Petreczky, et al., Phys. Rev. **D69**, 094507 (2004), hep-lat/0312037
12. A. Jakovac, P. Petreczky, K. Petrov, et al., Phys. Rev. **D75**, 014506 (2007), hep-lat/0611017
13. G. Aarts, C. Allton, M. B. Oktay, et al., Phys. Rev. **D76**, 094513 (2007), 0705.2198
14. H. Ding, A. Francis, O. Kaczmarek, et al., Phys.Rev. **D86**, 014509 (2012), 1204.4945
15. P. Petreczky, Eur.Phys.J. **C62**, 85 (2009), 0810.0258
16. A. Mocsy, P. Petreczky, Phys. Rev. **D77**, 014501 (2008), 0705.2559
17. F. Karsch, E. Laermann, S. Mukherjee, et al., Phys.Rev. **D85**, 114501 (2012), 1203.3770
18. R. Dowdall, et al. (HPQCD Collaboration), Phys.Rev. **D85**, 054509 (2012), 1110.6887
19. G. Aarts, S. Kim, M. Lombardo, et al., Phys.Rev.Lett. **106**, 061602 (2011), 1010.3725
20. G. Aarts, C. Allton, S. Kim, et al., JHEP **1111**, 103 (2011), 1109.4496
21. N. Brambilla, A. Pineda, J. Soto, et al., Nucl. Phys. **B566**, 275 (2000), hep-ph/9907240
22. N. Brambilla, A. Pineda, J. Soto, et al., Rev.Mod.Phys. **77**, 1423 (2005), hep-ph/0410047
23. N. Brambilla, J. Ghiglieri, A. Vairo, et al., Phys. Rev. **D78**, 014017 (2008), 0804.0993
24. M. Laine, O. Philipsen, P. Romatschke, et al., JHEP **0703**, 054 (2007), hep-ph/0611300
25. N. Brambilla, M. A. Escobedo, J. Ghiglieri, et al., JHEP **1009**, 038 (2010), 1007.4156
26. P. Petreczky, C. Miao, A. Mocsy, Nucl.Phys. **A855**, 125 (2011), 1012.4433
27. A. Rothkopf, T. Hatsuda, S. Sasaki, PoS **LAT2009**, 162 (2009), 0910.2321
28. A. Rothkopf, T. Hatsuda, S. Sasaki, Phys.Rev.Lett. **108**, 162001 (2012), 1108.1579
29. A. Bazavov, P. Petreczky (2012), 1210.6314
30. A. Bazavov, P. Petreczky (2012), 1211.5638
31. O. Jahn, O. Philipsen, Phys. Rev. **D70**, 074504 (2004), hep-lat/0407042
32. F. Zantow, O. Kaczmarek, F. Karsch, et al., Nucl.Phys.Proc.Suppl. **106**, 519 (2002), hep-lat/0110103
33. O. Kaczmarek, F. Karsch, P. Petreczky, et al., Phys. Lett. **B543**, 41 (2002), hep-lat/0207002
34. S. Digal, S. Fortunato, P. Petreczky, Phys. Rev. **D68**, 034008 (2003), hep-lat/0304017
35. O. Kaczmarek, F. Karsch, F. Zantow, et al., Phys.Rev. **D70**, 074505 (2004), hep-lat/0406036
36. A. Bazavov, P. Petreczky, A. Velytsky, Phys. Rev. **D78**, 114026 (2008), 0809.2062
37. P. Petreczky, K. Petrov, Phys. Rev. **D70**, 054503 (2004), hep-lat/0405009

38. O. Kaczmarek, F. Zantow, Phys. Rev. **D71**, 114510 (2005), [hep-lat/0503017](#)
39. O. Kaczmarek, PoS **CPOD07**, 043 (2007), [0710.0498](#)
40. P. Petreczky, J.Phys.G **G37**, 094009 (2010), [1001.5284](#)
41. P. Petreczky, Eur. Phys. J. **C43**, 51 (2005), [hep-lat/0502008](#)
42. N. Brambilla, J. Ghiglieri, P. Petreczky, et al., Phys.Rev. **D82**, 074019 (2010), [1007.5172](#)
43. Y. Burnier, M. Laine, M. Vepsalainen, JHEP **1001**, 054 (2010), [0911.3480](#)
44. M. Berwein, N. Brambilla, J. Ghiglieri, et al. (2012), [1212.4413](#)
45. A. Bazavov, T. Bhattacharya, M. Cheng, et al., Phys. Rev. **D85**, 054503 (2012), [1111.1710](#)
46. E. Follana, et al. (HPQCD Collaboration, UKQCD Collaboration), Phys. Rev. **D75**, 054502 (2007), [hep-lat/0610092](#)
47. M. Clark, A. Kennedy, Z. Sroczynski, Nucl. Phys. Proc. Suppl. **140**, 835 (2005), [hep-lat/0409133](#)
48. A. Bazavov, et al. (MILC collaboration), Phys. Rev. **D82**, 074501 (2010), [1004.0342](#)
49. A. Bazavov, et al. (MILC Collaboration), PoS **LATTICE2010**, 074 (2010), [1012.0868](#)
50. M. Albanese, et al. (APE), Phys. Lett. **B192**, 163 (1987)
51. A. Hasenfratz, F. Knechtli, Phys. Rev. **D64**, 034504 (2001), [hep-lat/0103029](#)
52. M. Cheng, N. Christ, S. Datta, et al., Phys. Rev. **D77**, 014511 (2008), [0710.0354](#)
53. M. Cheng, S. Ejiri, P. Hegde, et al., Phys. Rev. **D81**, 054504 (2010), [0911.2215](#)
54. W. Detmold, M. J. Savage, Phys.Rev.Lett. **102**, 032004 (2009), [0809.0892](#)
55. C. Aubin, C. Bernard, C. DeTar, et al., Phys. Rev. **D70**, 094505 (2004), [hep-lat/0402030](#)
56. W. Detmold, S. Meinel, Z. Shi (2012), [1211.3156](#)
57. O. Kaczmarek, F. Karsch, P. Petreczky, et al., Nucl.Phys.Proc.Suppl. **129**, 560 (2004), [hep-lat/0309121](#)

